

# Generation and Control of Ultrashort Supercontinuum Pulses

Franziska Kirschner, Mansfield College, University of Oxford

September 10, 2014



## Abstract

Supercontinuum laser pulses in the visible and near infrared region find themselves in a wide range of applications from biology to meteorology and their generation is a delicate procedure dependent on a variety of linear and nonlinear effects. Part of this project concerns the optimisation of the stability and spectral bandwidth of the supercontinuum pulses created by self-phase modulation in a hollow-core fiber. By modifying the experimental setup and using optimal energy and pressure conditions, a maximum bandwidth of  $(575 \pm 22)\text{nm}$  was achieved; similar to other SPM-induced bandwidths using different beam input parameters [1]. A primary requirement of supercontinuum applications is a constant peak amplitude of the pulse, determined by the carrier-envelope phase (CEP) amongst other factors. It is therefore vital to control the CEP in order to maintain a constant peak amplitude; one of the earliest methods involved the use of an f-to-2f interferometer [2], and one was built for later use on the Ti:Sapphire laser utilised in this project.

## Contents

<b>1</b>	<b>Introduction</b>	<b>2</b>
1.1	Creating ultrashort supercontinuum pulses . . . . .	2
1.2	CEP and f-to-2f interferometry . . . . .	2
<b>2</b>	<b>Experimental Setup</b>	<b>4</b>
2.1	Hollow Core Fiber . . . . .	4
2.2	f-to-2f interferometer . . . . .	5
<b>3</b>	<b>Results and Analysis</b>	<b>5</b>
3.1	Beam profile and spectrum . . . . .	5
<b>4</b>	<b>Conclusion</b>	<b>7</b>

# 1 Introduction

## 1.1 Creating ultrashort supercontinuum pulses

Supercontinuum ultrashort pulses are produced as a result of both linear and nonlinear optical effects. The main nonlinear phenomena involved in supercontinuum generation include self-phase modulation (SPM), four-wave mixing, intrapulse Raman scattering and soliton self-frequency shift [3]. In a hollow-core fiber (HCF) the predominant method of spectral broadening is via SPM [4], caused by the optical Kerr effect: the polarization in a dielectric medium is not proportional to the electric field at high intensities. This creates an instantaneous change in the refractive index

$$n(t, \vec{x}) = n_0 + n_2 I(t, \vec{x}), \quad (1)$$

where this change produces a phase shift in the highest intensity parts of the beam, with  $n_2$  of order  $10^{-16} \text{cm}^2/\text{W}$  [5]. The transverse and longitudinal components of the Kerr effect produce different nonlinearities in the beam, as can be seen in Figure 1, and this is a result of the third order nonlinearity in the optical susceptibility (a full derivation can be found in [6]).

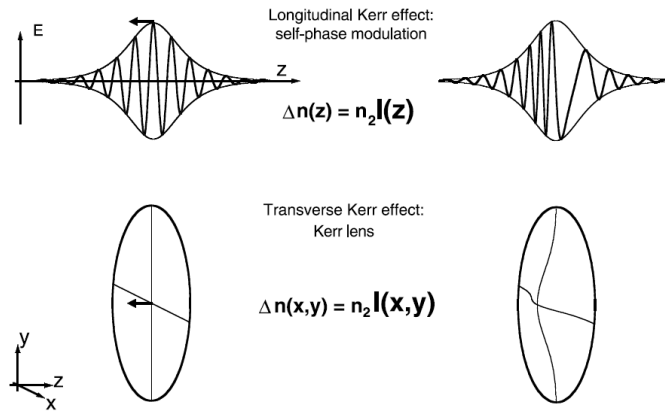


Figure 1: Transverse and longitudinal Kerr effect, taken from [5].

The transverse effect retards the most intense parts of the beam, acting like a focusing lens, whereas the longitudinal effect creates a red shift in the leading end of the pulse and a blue shift in the trailing end; this is SPM. The pulse can then be shortened using dispersion compensation, which advances the blue end of the pulse and delays the red end to remove any dispersion produced in the gas. For a pulse propagating over a distance  $L$  in a nonlinear medium, it picks up a phase

$$\Phi(t) = \frac{\omega}{c} n_2 I(t) L, \quad (2)$$

which, in the limit  $\frac{\partial I}{\partial t} \rightarrow \frac{I_0}{\tau}$  where  $I_0$  is the peak beam intensity and  $\tau$  is the pulse width, the maximum spectral broadening due to SPM is

$$\Delta\omega(t) = \frac{\omega}{c} n_2 L \frac{I_0}{\tau}. \quad (3)$$

From the Fourier transform of the broader frequency spectrum, a shorter pulse in the time domain is henceforth produced.

## 1.2 CEP and f-to-2f interferometry

In an optical pulse, the peak of the envelope and carrier waves may not necessarily align, causing a reduction in the peak intensity of the pulse. This phase difference between the two

waves is known as the carrier-envelope phase (CEP), also referred to as the ‘absolute phase’ [7], and causes the form of the pulse’s electric field to become

$$E(t) = A(t) \cos(\omega t + \phi), \quad (4)$$

where  $\phi$  is the CEP.

As the phase and group velocities of the pulses may not be equal (this can be caused by dispersion in optical components, as well as pressure and temperature fluctuations), the pulse-to-pulse CEP could vary. This change in the pulse-to-pulse CEP is known as the carrier-envelope offset (CEO). In the frequency domain, the corresponding offset frequency is related to the evolution of the CEP by

$$f_0 = \frac{1}{2\pi} \frac{d\phi}{dt}, \quad (5)$$

which in turn is related to the CEO ( $\delta\phi$ ) in the time domain by

$$\delta\phi = 2\pi \frac{f_0}{f_{\text{rep}}}, \quad (6)$$

where  $f_{\text{rep}}$  is the repetition frequency between pulses. From this it is clear that control of the CEO will result in control of the CEP, thus allowing a series of pulses with equal intensity to be produced.

One of the earliest methods for CEP control and measurement uses an f-to-2f interferometer, for which a typical design [7] is shown in Figure 2.

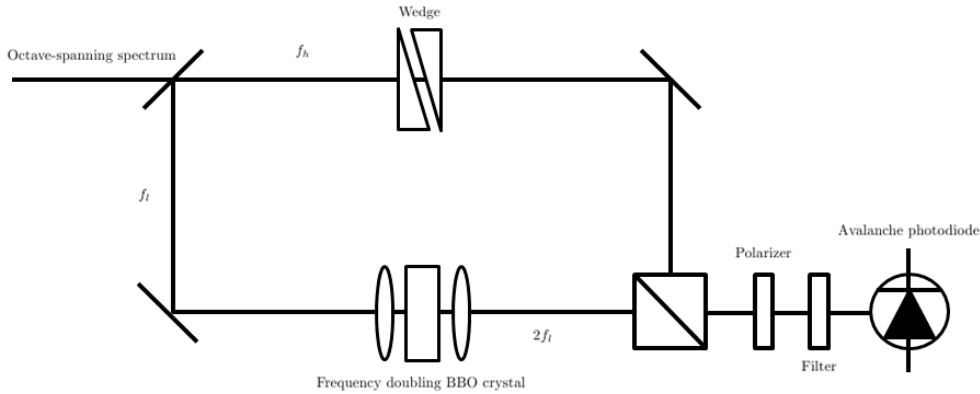


Figure 2: The f-to-2f interferometer.

In the frequency domain, the broadband pulses form a frequency comb with the  $n^{\text{th}}$  comb line represented by:

$$f_n = n f_{\text{rep}} + f_0, \quad (7)$$

and so by looking at the frequency spacing between two combs of differing  $n$ , it is possible to find the CEO frequency. The f-to-2f interferometer does this by referencing an octave-spanning source with itself, firstly by splitting it into low and high frequency components  $f_l$  and  $f_h$  respectively, where  $h = 2l$ . The low frequency component is then passed through a frequency doubling crystal, with an output of  $2f_l$ . Next, the offset frequency can be calculated by the difference between the

two interfering frequency combs at the avalanche photodiode:

$$f_h = 2lf_{\text{rep}} + f_0, \quad (8a)$$

$$f_l = lf_{\text{rep}} + f_0, \quad (8b)$$

$$2f_l - f_h = f_0. \quad (8c)$$

In a mode-locked laser, the interferometer is connected to a feedback loop to allow for effective CEP control.

## 2 Experimental Setup

### 2.1 Hollow Core Fiber

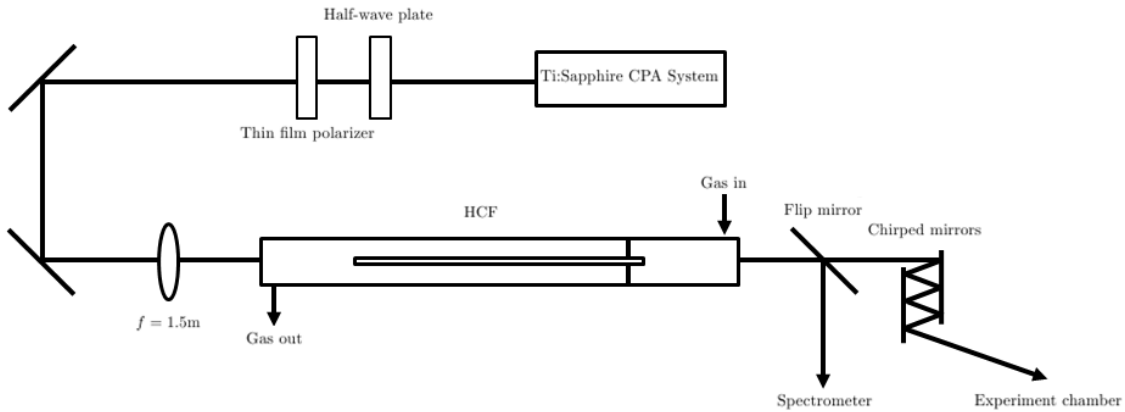


Figure 3: Setup for broadband generation in the HCF.

A HCF was used to generate a broadband spectrum from the Ti:Sapphire laser. It was enclosed in an isolated tube, and a pressure gradient of a noble gas was run through the fiber to produce the nonlinear refractive index, as shown in Figure 3. The pressure gradient was chosen to compromise between the need for beam stability at the entrance of the fiber (which is optimal in a vacuum), minimisation of energy loss due to absorption by the gas, and the high gas pressure required for supercontinuum generation. An adjustable half-wave plate and polarizing filter were included to allow control over the input beam energy in the HCF. Several modifications were made to the previous setup in order to maximise broadening and minimise energy loss, including:

- the lens to focus the laser beam at the entrance of the HCF was replaced to shorten the focal length and produce a smaller beam diameter at the HCF entrance,
- the first part of the HCF tube (which did not contain the fiber) was replaced to reduce the overall length of the tube to accommodate the shortened focal length,
- the windows at the front and rear of the HCF tube was replaced to reduce its thickness, minimising the nonlinearities and dispersion produced from the propagation of the beam through glass;
- a thicker tube was used to connect the vacuum pump to the HCF tube, to increase the pump's power;
- Ar was used for the pressure gradient instead of Ne, as it has a lower first ionisation energy and thus will produce a broader spectrum, and
- blue and green chirped mirrors were used to compensate for the phase difference between the red and blue ends of the light, removing any dispersion in the pulse.

## 2.2 f-to-2f interferometer

The interferometer was constructed as in Figure 2, using silver mirrors and a 400nm filter.

## 3 Results and Analysis

### 3.1 Beam profile and spectrum

The spectrum was initially measured with an input energy of 1.30mJ, output energy of 0.96mJ and HCF output pressures between 100mbar and 500mbar. It was found that the spectrum broadened with increased pressure gradient (as shown in Figure 4), as expected due to the increasing nonlinear susceptibility. An exponential fit and a linear fit were applied to the graph, but it is unclear as to which pattern the data follow. This could be due to the low range of data points; if the data only forms part of a larger exponential curve it could be approximated as linear. Both fits did not pass through the origin, which is expected as the laser output spectrum is not a delta function, so broadening exists even in the absence of SPM.

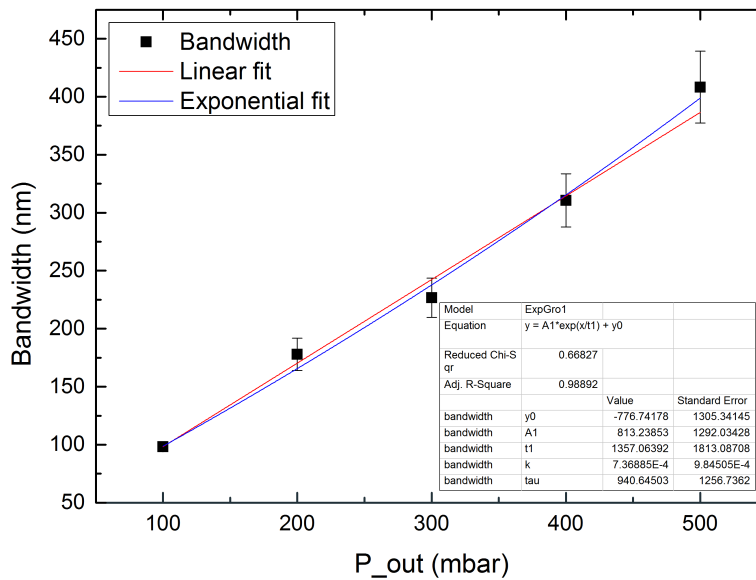


Figure 4: Spectral bandwidths for  $E_{in} = 1.30\text{mJ}$ ,  $E_{out} = 0.96\text{mJ}$ ,  $P_{in} = 0\text{mbar}$ , with exponential fit parameters.

A problem with this measurement is the high energy, which caused a large instability in the beam profile. This created large errors in the data and meant high pressure gradient measurements were impossible. For this reason, the measurements were repeated with a lower input energy of 0.60mJ and output energy of 0.45mJ. This showed a much more stable beam profile over a larger range of pressure gradients, meaning a larger supercontinuum was achievable with a maximum bandwidth of  $(575 \pm 22)\text{nm}$ . The bandwidths from this experiment can be seen in Figure 5. It was chosen not to include results from higher or lower pressure gradients, as very low gradients were not sufficient to induce SPM at such a low energy, and high gradients caused the beam to become very unstable. An exponential fit was once again applied, and it worked well. These results do not appear to also follow a linear progression, which is likely due to the larger range of the data set. The wide variation in spectral bandwidth can also be seen in Figure 6, where the spectra for the minimum and maximum  $P_{out}$  are compared; the bandwidth was seen to increase by  $(429 \pm 26)\text{nm}$ .

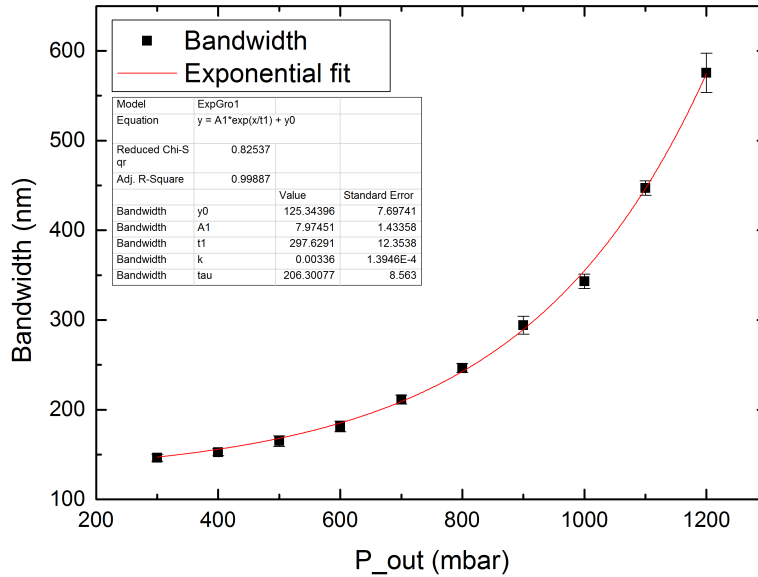


Figure 5: Spectral bandwidths for  $E_{in} = 0.60\text{mJ}$ ,  $E_{out} = 0.45\text{mJ}$ ,  $P_{in} = 0\text{mbar}$ , with exponential fit parameters.

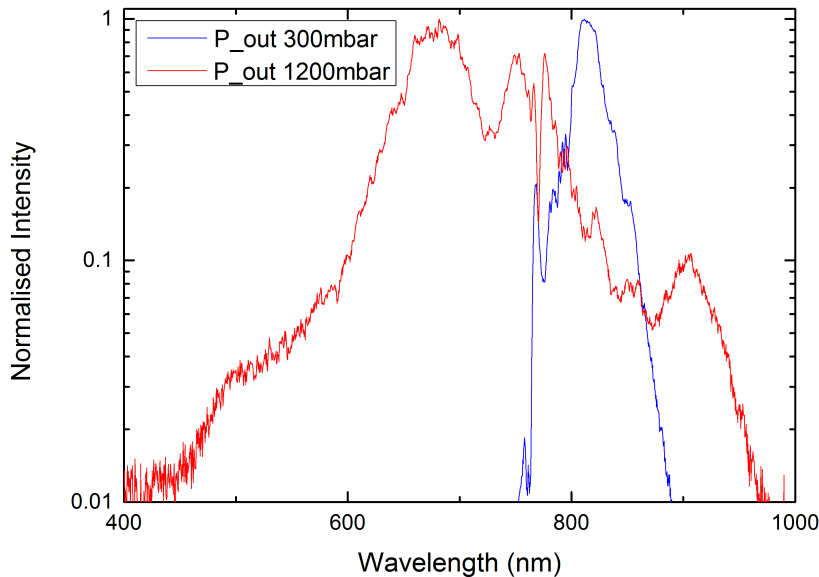


Figure 6: Spectra for  $E_{in} = 0.60\text{mJ}$ ,  $E_{out} = 0.45\text{mJ}$ ,  $P_{in} = 0\text{mbar}$  at high and low  $P_{out}$ .

Despite both data sets following close to an exponential distribution, their fitting parameters are very different. This could suggest that these parameters are energy-dependent, or that the data follows another, non-exponential distribution.

The effectiveness of the vacuum pump was also investigated; clearly it is impossible to have  $P_{in} = 0$ , and the results are displayed in Figure 7 for both argon and neon. It was found that at high pressures  $P_{in}$  seemed to decrease linearly, but after a minimum at 800mbar  $P_{in}$  was seen to increase linearly for both gases. A possible reason for this could be the play-off between higher gas

input pressure versus the power of the pump. As the pump's power decreases with input pressure [8], a point must be reached when the pump's power is so low that it can no longer facilitate the higher vacuum produced for lower input gas pressures. It can also be seen, however, that all  $P_{in}$  values remain below 0.1% of the corresponding  $P_{out}$ , so it is safe to assume a total vacuum at the beam input of the HCF.

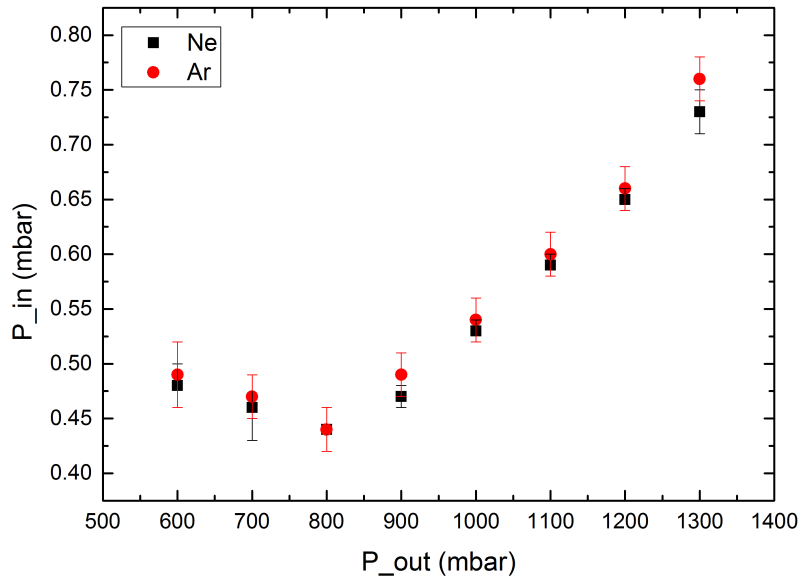


Figure 7: Variation in beam input pressure with beam output pressure.

## 4 Conclusion

This project included modifying the HCF setup to improve its production of supercontinuum femtosecond pulses, and the construction of an f-to-2f interferometer.

First, the experimental equipment was exchanged in order to optimise energy transmission and beam stability. The main aims of this were to reduce the thickness of glass the beam travelled through (to reduce the effect of uncontrollable nonlinearities), minimise the beam diameter at the entrance to the HCF to ensure optimal transmission through the fiber, and effectively shield the beam from any causes of disturbance (for example air and mechanical movement). The modifications listed under Experimental Setup were found to significantly improve the output beam, so that optimal conditions for SPM could be sought. With beam stability still in mind, it was seen that a lower input energy resulted in drastic improvements in the range of pressure gradients that could be used. Using an input energy of 0.60mJ, output energy of 0.45mJ, input pressure of 0mbar, and output pressure of 1200mbar, a maximum spectral width of  $(575 \pm 22)$ nm was produced. The effectiveness of the vacuum pump was also investigated, and it was seen that the assumption of  $P_{in} = 0$ mbar is justified.

The next step in this stabilisation is to revert the gas back to Ne, to allow higher energies and gradients to be used stably. Another option is to use induced-pulse modulation to generate broader spectra [9].

The construction and alignment of the f-to-2f interferometer was successful, and it will be used in the future to monitor the CEP stability of the Ti:Sapphire laser used with the HCF. Along with this, the next steps in this experiment will involve the compression of the pulse and measurement of the pulse duration using a FROG [10]. Afterwards, the output beam will be redirected in order to be used in high harmonic generation [11] and further experiments.

## Acknowledgements

I would like to thank my supervisor, Shaobo Fang, for his guidance and support in this fascinating and fun project. I give also thanks to the rest of the Ultrafast Optics and X-rays Division at CFEL for getting me through long days in the lab and for all of the knowledge they have imparted upon me. DESY, its summer school, and the organisers also receive many thanks. Finally, I would like to give my utmost gratitude to Lidl, without which I probably would not have eaten for the past 7 weeks.

## References

- [1] S. Bohman, A. Suda, T. Kanai, S. Yamaguchi, K. Midorikawa, *Optics Letters*, **35**, pp. 1887-1889 (2010).
- [2] H. R. Telle, G. Steinmeyer, A. E. Dunlop, J. Stenger, D. H. Sutter, U. Keller, *Appl. Phys. B*, **69**, pp. 327-332 (1999).
- [3] W. T. Mohamed, J. An, D. E. Kim, *Selected Topics on Optical Fiber Technology*, ch. 7 (2012).
- [4] A. Hasegawa, F. Tappert, *Appl. Phys. Lett.* **23**, 142 (1973).
- [5] G. Steinmeyer, D. H. Sutter, L. Gallmann, N. Matuschek, U. Keller, *Science*, **286**, 5444 (1999).
- [6] G. New, *Introduction to Nonlinear Optics*, Cambridge University Press (2014).
- [7] Z. Wei, H. Han, W. Zhang, Y. Zhao, J. Zhu, H. Teng, Q. Du, *Advances in Solid-State Lasers: Developments and Applications*, ch. 14 (2010).
- [8] Technical Specifications for nXDS10i vacuum pump, *edwardsvacuum.com* <https://www.edwardsvacuum.com/Products/View.aspx?sku=A73601983>.
- [9] N. Karasawa, R. Morita, H. Shigekawa, M. Yamashita, *Optics Letters*, **25**, pp. 183-185 (2000).
- [10] R. Trebino, K. W. DeLong, D. N. Fittinghoff, J. N. Sweetser, M. A. Krumbügel, B. A. Richman, D. J. Kane, *Rev. Sci. Instrum.* **68**, 3277 (1997).
- [11] K. -H. Hong, C. -J. Lai, V. -M. Gkortsas, S. -W. Huang, J. Moses, E. Granados, S. Bhardwaj, F. X. Kärtner, *Phys. Rev. A*, **86**, 043412 (2012).